JACS
JOURNAL OF THE AMERICAN CHEMICAL SOCIETY
Communication
pubs.acs.org/JACS

Nitrogen-Doped Fullerene as a Potential Catalyst for Hydrogen Fuel Cells

Feng Gao,[†] Guang-Lin Zhao,*[,†] Shizhong Yang,[‡] and James J. Spivey[§]

[†]Department of Physics and [‡]Department of Computer Science, Southern University and A&M College, Baton Rouge, Louisiana 70813, United States

[§]Department of Chemical Engineering, Louisiana State University, Baton Rouge, Louisiana 70803, United States

Supporting Information

ABSTRACT: We examine the possibility of nitrogen-doped C_{60} fullerene (N-C_{60}) as a cathode catalyst for hydrogen fuel cells. We use first-principles spin-polarized density functional theory calculations to simulate the electrocatalytic reactions on N-C_{60}. The first-principles results show that an O_2 molecule can be adsorbed and partially reduced on the N−C complex sites (Pauling sites) of N-C_{60} without any activation barrier. Through a direct pathway, the partially reduced O_2 can further react with H^+ and additional electrons and complete the water formation reaction (WFR) with no activation energy barrier. In the indirect pathway, reduced O_2 reacts with H^+ and additional electrons to form H_2O molecules through a transition state (TS) with a small activation barrier (0.22−0.37 eV). From an intermediate state to a TS, H^+ can obtain a kinetic energy of ∼0.95−3.68 eV, due to the Coulomb electric interaction, and easily overcome the activation energy barrier during the WFR. The full catalytic reaction cycles can be completed energetically, and N-C_{60} fullerene recovers to its original structure for the next catalytic reaction cycle. N-C_{60} fullerene is a potential cathode catalyst for hydrogen fuel cells.

Precious platinum catalyst is a key ingredient for hydrogen fuel cells, which are an attractive energy technology for mobile and stationary applications. They are environmentally friendly, producing low emissions and exhibiting high energy conversion efficiency and high power density.[1−3] However, Pt is rare and expensive. Reducing the amount of Pt loading by identifying new non-precious-metal catalysts is a major target in the current research for these new technologies. Developing alternative catalysts to substitute Pt for oxygen reduction reaction (ORR) is essential, because the slow kinetics of the ORR can cause significant efficiency losses in fuel cells. Ozkan et al. reported that N-containing nanostructured carbons and nanotubes have promising catalytic activity toward ORR.[4,5] Yang et al. prepared vertically aligned carbon nanotubes (ACNTs) using a versatile chemical vapor deposition method and demonstrated that ACNTs functionalized through N- and Fe-doping can be electrocatalytically active for ORR.[6] Dai et al. reported that vertically aligned nitrogen-containing carbon nanotubes (VA-NCNTs) can act as metal-free electrode catalysts toward ORR through a four-electron pathway.[7] N-doped graphene has also been studied as a potential cathode catalyst for fuel cells with promising electrocatalytic properties toward ORR.[8−10] Wu et al. reported N-enriched FeCo core-carbon graphitic shell structures that catalyze the ORR with high activity and remarkable performance stability for non-precious-metal catalysts.[11]

Azafullerenes, in which one or more cage carbons are substituted by N atoms, also show tunable chemical and physical properties.[12] With N-doping into the cage structure of fullerene, charge transfer (CT) occurs between the N and C atoms, resulting in an unbalanced charge distribution in the azafullerene. This makes the N−C complex site in N-doped fullerene preferential for electrophilic and nucleophilic attack.[13] Experimentally, N-doped fullerenes can be prepared by vaporization of graphite in N-containing atmosphere or condensed-phase organic synthesis. Otero et al. reported the formation of triazafullerene $C_{57}N_3$ from aromatic precursors using a highly efficient surface-catalyzed cyclodehydrogenation process.[14] Hultman et al. successfully synthesized cross-linked solid nano-onions of carbon nitride by a reactive magnetron sputtering method.[15] Electron microscopy and energy loss spectroscopy show that the core-shells contain up to 20% N substitution, corresponding to $C_{48}N_{12}$. Based on B3LYP/6-31G* level density functional calculations, Manaa et al. demonstrated the stability of $C_{48}N_{12}$ azafullerene.[16,17] Using linear density functional theory (DFT) based on ab initio calculations employing BLYP exchange interactions, Sharma et al. calculated the detailed structural, electronic, and vibrational properties of $C_{60-n}N_n$ (n = 1−12).[13] They also explored the possibility of trapping polynitrogen clusters inside C_{60} fullerene using DFT calculations.[18]

Here we report our recent studies on the electrocatalytic properties of nitrogen-doped C_{60} fullerene (N-C_{60}) as a potential cathode electrode catalyst for hydrogen fuel cells. We studied the ORR on N-C_{60} using first-principles spin-polarized DFT calculations. We further studied the elementary catalytic reaction steps, reaction pathways, and activation energy barriers (E_a) for the water formation reaction (WFR) on N-C_{60}, which are keys to understanding electrocatalytic reactions on the cathode of fuel cells. We identified that the N−C complex sites (Pauling sites) on N-C_{60} are catalytic sites, and that full-cell electrocatalytic reactions can be realized through direct pathways (DPWs) with E_a = 0 or through indirect pathways (IDPWs) with low $E_a \approx$ 0.22−0.34 eV.

Received: September 11, 2012
Published: September 19, 2012

dx.doi.org/10.1021/ja309042m | J. Am. Chem. Soc. 2013, 135, 3315−3318

We performed first-principles spin-polarized DFT calculations using the Vienna ab initio simulation package, which implements the plane-wave pseudopotential method.[19−21] Projector-augmented plane wave[22,23] potentials were employed. The exchange-correlation interaction potentials and energies were described by a formalism developed by Ceperly and Adler in local density approximation.[24] A plane wave basis set was used with an energy cutoff of 400 eV. A supercell method was used to simulate N-C_{60} fullerene and interactions with O_2 and H atoms, with a cell size of 16 × 16 × 16 Å^3. In the supercell method, Gamma point was used for the total energy calculations. In the self-consistent DFT calculations, the total energy converged to $<1 \times 10^{-5}$ eV. The atomic positions were fully relaxed in all the DFT calculations until the residue forces were <0.05 eV/Å on the atoms. In this work, we studied substitutional N-doping in C_{60} fullerene: a C atom is substituted by an N atom while retaining the C_{60} fullerene structure. Substitutional N-doping is the most-often identified type of N-doping in C_{60} fullerenes.[13−17,25,26] N-doping on the fullerene creates two types of N−C atomic sites (Pauling sites): a C−N complex site between two hexagonal rings (HH Pauling site), and a C−N site connecting a hexagonal ring and a pentagonal ring (HP Pauling site). The structures and N−C bond lengths of the HH and HP Pauling sites are displayed in Figure S1. We studied ORR and WFR on both Pauling sites. Studies of ORR on N-C_{60} aimed to simulate the half-cell reaction on the cathode of a hydrogen fuel cell. Studies of WFR and related reaction pathways on N-C_{60} aimed to understand the full-cell reaction on the cathode of a hydrogen fuel cell. The adsorption energy (E_{ads}) of ORR can be determined by

$$E_{ads} = E_{\text{N-}C_{60}O_2} - E_{\text{N-}C_{60}} - E_{O_2} \quad (1)$$

where $E_{\text{N-}C_{60}}$ and $E_{\text{N-}C_{60}O_2}$ denote the total energies of N-C_{60} before and after O_2 adsorption, respectively, and E_{O_2} is the total energy of free O_2. The minimum energy pathways (MEPs) of the reactions were calculated by using the nudged elastic band (NEB) method.[27−29]

Figure 1a shows the MEP of O_2 adsorption and reduction on the HH Pauling site of N-C. There is no activation energy barrier

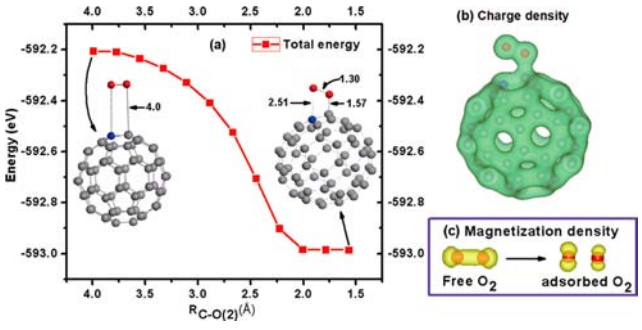

Figure 1. (a) Minimum energy path for ORR on the HH Pauling site of N-C_{60}. Embedded are relaxed structures of O_2 on the N-C_{60} before and after the ORR. (b) Three-dimensional charge density distribution of N-C_{60} with O_2 adsorption. (c) Three-dimensional magnetization density of O_2 before and after adsorption. Gray, blue, red, and white spheres represent C, N, O, and H atoms, respectively.

for this process. The calculated E_{ads} for O_2 on the HH Pauling site is −0.83 eV. The images in Figure 1a show the relaxed structures of N-C_{60} before and after O_2 reduction. O_2 is adsorbed onto the HH Pauling site by forming a C−O bond. In the following discussions, O(1) refers to the oxygen atop the N atom, and O(2) refers to an oxygen bonded to a C atom at the Pauling sites. After O_2 adsorption, a C−O(2) bond is formed with a bond length of ∼1.57 Å, and the N−O(1) distance is 2.51 Å. The O_2 reduction on N-C_{60} can be described by three major physical quantities, based on the results of the first-principles spin-polarized DFT calculations: (1) The extension of O−O bond length, which is increased to 1.30 Å. The DFT-calculated O−O bond length for free O_2 is 1.22 Å, which is nearly the same as the experimental value of 1.21 Å. The results indicate that the O−O bond becomes weaker due to the reduction of O_2. (2) Thecalculated charge transfer, wherein the two O atoms become $O(1)^{-0.17}$ and $O(2)^{-0.25}$, respectively. The effective charges and CTs for the system are evaluated by Bader charge analysis using the code developed by Henkelman et al.[30] (3) The change of the magnetic moment of the O_2 molecule, which is reduced to 0.99 μ_B from 2.0 μ_B in the case of a free O_2 molecule.

Figure 1b displays the 3-D iso-surfaces (with an iso-density value of 0.1 e/Å^3) of electron density (spin-up plus spin-down) of N-C_{60} with O_2 adsorbed onto the HH Pauling site. The overlap of the electron densities of O(2) and the C atom indicates the formation of a new bond between the C atom and O(2). Figure 1c shows the 3-D iso-surfaces (with an iso-density value of 0.05 e /Å^3) of magnetization density (which is defined as spin-up density minus spin-down density) of O_2 before and after adsorption on the HH Pauling site of N-C_{60}. It clearly shows that the magnetization density in the region between the two O atoms is substantially reduced when an O_2 molecule is absorbed onto the HH Pauling site. The calculated magnetic moments of O(1) and O(2) for the reduced O_2 are 0.61 and 0.38 μ_B, respectively, much smaller than the magnetic moment of 1.0 μ_B per O atom for the case of a free O_2 molecule.

As pointed out by Kaukonen et al.,[31] high catalytic activity on the cathode electrode of hydrogen fuel cells through ORR should fulfill at least three criteria. First, it should have the lowest formation energy possible. Second, it should bind O_2 with relatively low binding energy. Third, the energy barrier for O_2-binding with protons and electron additions for the WFR should not be too high. In fact, ORR is only the half-cell reaction. The third criterion is related to the fulfillment of the full-cell reaction on the cathode of hydrogen fuel cells.

We further performed a series of first-principles spin-polarized DFT calculations to examine the possibilities of the WFR after ORR on the HH and HP Pauling sites of N-C_{60} fullerene. We found that there are two possible pathways through which the reduced O_2 reacts with protons and electron additions in forming free H_2O molecules. One is the DPW, in which two protons nearly simultaneously approach a reduced O with two additional electrons and then form a H_2O molecule that desorbs from the catalytic site. The other possibility is the IDPW, through which an intermediate state of OH forms at the catalytic site and subsequently a second H approaches to OH, forming a H_2O molecule with an activation energy barrier.

Figure 2a shows the MEP for the interaction steps of O(1) with two H^+ and two additional electrons through a DPW on the HH Pauling site of N-C_{60} fullerene. The embedded images show the atomic structures of the initial, intermediate, and final states of the reaction. The initial state shows that two H atoms are 3.0 Å from O(1) with a H−O(1)−H angle of 104.5°. As long as the two H atoms reach a distance of ∼1.5 Å from O(1) (an intermediate state), they react with O(1) and form a H_2O molecule. The bond length and bond angle in the formed H_2O are 0.97 Å and 104.4°, respectively, close to those values for a free H_2O molecule (0.98 Å and 104.5°, respectively). Due to

dx.doi.org/10.1021/ja309042m | J. Am. Chem. Soc. 2013, 135, 3315−3318

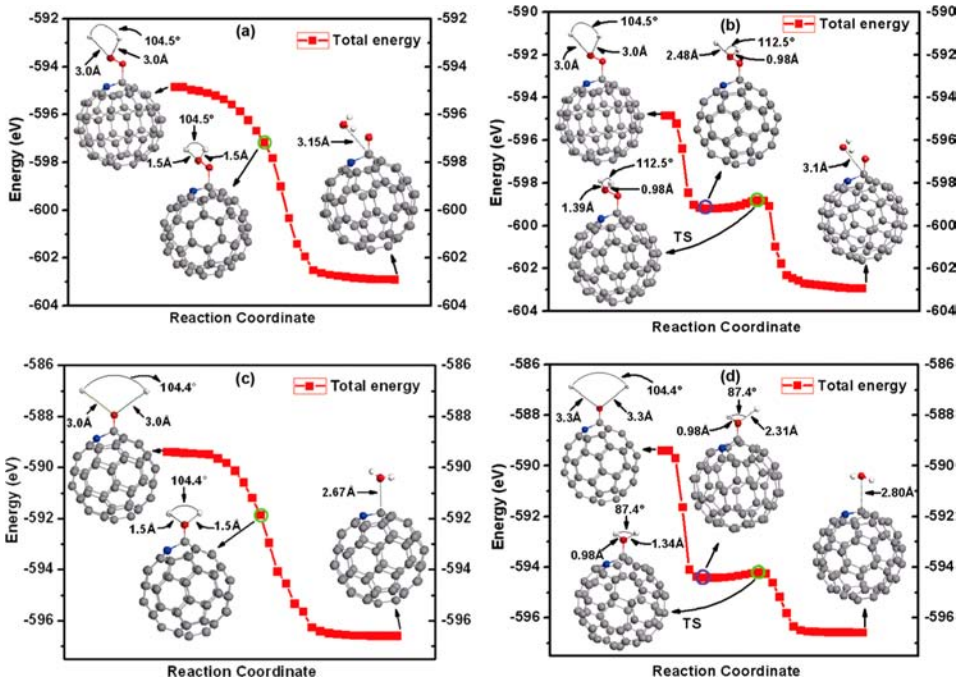

Figure 2. Minimum energy paths for H_2O formation on O(1) through (a) a direct pathway and (b) an indirect pathway, and on O(2) through (c) a direct pathway and (d) an indirect pathway, on the HH Pauling site of N-C_{60} fullerene. Embedded images show the atomic structures of the initial, intermediate, and final states of the reactions.

Coulomb repulsion between O(2) and H_2O, the H_2O molecule desorbs from the catalytic site (the final state). There is no activation energy barrier for the DPW in the WFR.

Figure 2b shows an IDPW for the interaction of O(1) with two H^+'s and two additional electrons on the HH Pauling site. It is possible that one of the two H atoms moves toward O(1) first and forms O−H, which is an intermediate state. The O−H bond length is 0.98 Å. The second H has to overcome E_a = 0.37 eV through a transition state (TS), which has the maximum total energy among the nearby reaction configurations, as shown in Figure 2b, moving close to the O−H and forming a H_2O. Once the H_2O molecule is formed, it desorbs from the catalytic site (the final state). Further, we calculated the vibrational frequencies of the H^+'s at the TS. In the harmonic approximation, there is only one imaginary frequency which is related to the vibration of H^+ along the MEP for the WFR of H_2O(l) (see Table S2). The results confirmed that the TS derived from the NEB calculation is a saddle point. In the intermediate state, Bader charge analysis shows O(1) becoming $O(1)^{-1.0}$. When a H^+ moves close to O(1)−H, from the intermediate state to the TS, there is a potential energy change of ∼1.21 eV due to the Coulomb electric interaction. This change of the potential energy will transfer to the kinetic energy of H^+ that is not included in the DFT calculation which was done essentially at T = 0 K. The kinetic energy (∼1.21 eV) of the H^+, when it reaches the TS, can easily overcome the E_a (0.37 eV) during the WFR through IDPW.

To confirm that the HH Pauling site is fully recovered after the ORR and WFR on O(1), we further simulated the WFR on O(2). Figure 2c shows the MEP for the H_2O formation on O(2) through a DPW on the HH Pauling site of the N-C_{60} fullerene. The embedded images show the atomic structures of the initial, intermediate, and final states of the reaction. There is no activation energy barrier for the DPW process. Two H's approach O(2) and form H_2O, which then desorbs from the catalyst site. The N-C_{60} recovers back to its original structure, and a full-cell catalytic reaction is completed. The HH Pauling site of N-C_{60} can serve for the next catalytic reaction cycle.

Figure 2d shows that O(2) can also react with two H^+'s through IDPW in forming a H_2O molecule, which desorbs from the adsorbent. At the intermediate state, the O−H bond length is 0.98 Å. There is a TS between the intermediate and final states, in which the H−O(2) distance is 1.34 Å and the total energy has a local maximum. The TS was also confirmed by calculations of the vibrational frequencies of H^+. The calculated results show that, at the TS, the vibration associated with H^+ has only one imaginary frequency, which is along the calculated MEP (Table S2). For the IDPW E_a = 0.21 eV, which is smaller than the case of WFR on O(1) through the same reaction. Bader charge analysis shows a negative charge of $O(2)^{-1.66}$ at the TS in Figure 2d. As we discussed above for the WFR on O(1), a H^+ moving from the intermediate state to TS on O(2) can obtain a kinetic energy of ∼3.49 eV. This kinetic energy of H^+ can easily overcome the E_a of 0.21 eV in the WFR through IDPW on O(2).

We repeated the same calculation procedure for ORR and WFR on the HP Pauling site of N-C_{60} fullerene. The calculated MEP also shows no activation energy barrier for the ORR on the HP site. After O_2 adsorption, the C−O(2) bond length is 1.62 Å. The N−O(1) distance is 2.48 Å. The O−O bond is increased to 1.29 Å, due to a partial reduction of O_2. The calculated CTs of the two O atoms are $O(1)^{-0.18}$ and $O(2)^{-0.25}$, respectively. The magnetic moment of O_2 is reduced to 0.94 μ_B. For the ORR at the HP Pauling site, E_{ads} = −0.31 eV, which is smaller than that on the HH Pauling site. We also studied the WFR on the HP Pauling site through DPW and IDPW processes. Through the DPW on the HP Pauling site, the calculated MEPs show no activation energy barrier for the formation of H_2O molecules. WFRs can also be achieved through IDPW on the HP Pauling site, which needs to overcome E_a = 0.22 and 0.29 eV, respectively, for the formations of the first and second H_2O. We also repeated the

dx.doi.org/10.1021/ja309042m | J. Am. Chem. Soc. 2013, 135, 3315−3318

calculations for the kinetic energy of H^+ in moving from the intermediate state to TS in the WFR for O(1) and O(2) through IDPW. They are 0.95 and 3.68 eV, respectively, much higher than the corresponding E_a. These results indicate that WFR steps for O(1) and O(2) through IDPW on the HP Pauling site can also be achieved. More details of the results are included in the Supporting Information.

We also investigated the possibilities of ORR on four other potential adsorption sites in N-C_{60}: the HH C−C site, the HP C−C site, the long bridge site, and the short bridge site (as shown in Figure S1). The HH C−C and HP C−C sites are away from doped N. The calculated MEPs for the ORR show E_a = 0.66 and 0.044 eV on the HH C−C site and HP C−C site, respectively. ORR on the HH C−C and HP C−C sites is not as favorable as that on the HH and HP Pauling sites. The first-principles results show that O_2 adsorption and reduction on the long bridge site and short bridge site are also not favorable as compared with those on the HH and HP Pauling sites. (See more details in the Supporting Information.)

We further examined the electrocatalytic properties of carbon fullerene with high N-doping. We performed spin-polarized DFT calculations for $C_{48}N_{12}$ fullerene, which has 12 N atoms substituting C atoms. We applied the same computation procedures as discussed above for ORR and WFR on the HP Pauling site of $C_{48}N_{12}$. The calculated results show that the properties of the full catalytic reaction cycle on the HP Pauling site of $C_{48}N_{12}$ are consistent with those of the single N-doping on C_{60} fullerene as discussed above. The ORR on the HP Pauling site of $C_{48}N_{12}$ is slightly stronger than those cases on N-C_{60}. This can be seen from the calculated values of the O−O bond length, the magnetic moment, and the CT in O_2 after ORR. The activation energy barrier for the WFR through IDPW on the Pauling site of $C_{48}N_{12}$ is also slightly lower than those cases on N-C_{60} (more details in Supporting Information, Tables S1 and S2). These results show that the electrocatalytic reaction is closely related to the local atomic structures, such as the N−C complex sites (Pauling site), and the atomic structures far away from the local catalytic site make an insignificant contribution. Various N-dopings into carbon fullerenes may be realized experimentally and can be used as potential cathode catalysts for hydrogen fuel cells.

In conclusion, by utilizing first-principles spin-polarized DFT calculations, we simulated the full-cell electrocatalytic reaction process on N-doped C_{60} fullerene. It was found that O_2 can be chemisorbed and partially reduced on the HH and HP Pauling sites of N-C_{60}. Through direct and indirect pathways, the partially reduced O_2 can further react with H^+ and additional electrons, forming H_2O molecules. The full catalytic reaction cycles can be completed energetically, and N-C_{60} fullerene recovers to its original structure for the next catalytic reaction cycle. The identified catalytic sites are HH and HP Pauling sites on N-C_{60}. These results indicate that N-C_{60} fullerene is a potential cathode catalyst for hydrogen fuel cells.

■ ASSOCIATED CONTENT

Supporting Information

Six figures and two tables providing the ORR and WFR data on the Pauling sites of N-C_{60} fullerene and $C_{48}N_{12}$. This material is available free of charge via the Internet at http://pubs.acs.org.

■ AUTHOR INFORMATION

Corresponding Author

guang-lin_zhao@subr.edu

Notes

The authors declare no competing financial interest.

■ ACKNOWLEDGMENTS

The work was funded in part by the National Science Foundation (NSF) LASIGMA Project (EPS-1003897, NSF92010-15-RII-SUBR), AFOSR (FA9550-09-1-0367), NSF project (CBET-0754821), and by DOE (DE-FE0003693, DE-FE0004734, DE-FE0007220, and DE-FE0008382). All the computations were performed on Louisiana Optical Network Initiative (LONI) computers. J.J.S. is supported by the Center for Atomic-level Catalyst Design, a DOE Energy Fronteir Research Center (DE-SC0001058).

■ REFERENCES

(1) Winter, M.; Brodd, R. J. *Chem. Rev.* **2004**, *104*, 4245.
(2) Joo, S. H.; Choi, S. J.; Oh, I.; Kwak, J.; Liu, Z.; Terasaki, O.; Ryoo, R. *Nature* **2001**, *412*, 169.
(3) Zhang, J.; Yang, H.; Fang, J.; Zou, S. *Nano Lett.* **2010**, *10*, 638.
(4) Matter, P.; Ozkan, U. *Catal. Lett.* **2006**, *109*, 115.
(5) Matter, P. H.; Zhang, L.; Ozkan, U. S. *J. Catal.* **2006**, *239*, 83.
(6) Yang, J.; Liu, D. J.; Kariuki, N. N.; Chen, L. X. *Chem. Commun.* **2008**, 329.
(7) Gong, K.; Du, F.; Xia, Z.; Durstock, M.; Dai, L. *Science* **2009**, *323*, 760.
(8) Qu, L.; Liu, Y.; Baek, J. B.; Dai, L. *ACS Nano* **2010**, *4*, 1321.
(9) Sheng, Z. H.; Shao, L.; Chen, J. J.; Bao, W. J.; Wang, F. B.; Xia, X. H. *ACS Nano* **2011**, *5*, 4350.
(10) Kim, H.; Lee, K.; Woo, S. I.; Jung, Y. *Phys. Chem. Chem. Phys.* **2011**, *13*, 17505.
(11) Wu, G.; More, K. L.; Johnston, C. M.; Zelenay, P. *Science* **2011**, *332*, 443.
(12) Chen, Z.; King, R. B. *Chem. Rev.* **2005**, *105*, 3613.
(13) Sharma, H.; Garg, I.; Dharamvir, K.; Jindal, V. K. *J. Phys. Chem. A* **2009**, *113*, 9002.
(14) Otero, G.; Biddau, G.; Sanchez-Sanchez, C.; Caillard, R.; Lopez, M. F.; Rogero, C.; Palomares, F. J.; Cabello, N.; Basanta, M. A.; Ortega, J.; Mendez, J.; Echavarren, A. M.; Perez, R.; Gomez-Lor, B.; Martin-Gago, J. A. *Nature* **2008**, *454*, 865.
(15) Hultman, L.; Stafström, S.; Czigány, Z.; Neidhardt, J.; Hellgren, N.; Brunell, I. F.; Suenaga, K.; Colliex, C. *Phys. Rev. Lett.* **2001**, *87*, 225503.
(16) Manaa, M. R.; Sprehn, D. W.; Ichord, H. A. *J. Am. Chem. Soc.* **2002**, *124*, 13990.
(17) Manaa, M. R. *Solid State Commun.* **2004**, *129*, 379.
(18) Sharma, H.; Garg, I.; Dharamvir, K.; Jindal, V. K. *J. Phys. Chem. C* **2010**, *114*, 9153.
(19) Kresse, G.; Furthmüller, J. *Comput. Mater. Sci.* **1996**, *6*, 15.
(20) Kresse, G.; Furthmüller, J. *Phys. Rev. B* **1996**, *54*, 11169.
(21) Kresse, G.; Hafner, J. *Phys. Rev. B* **1993**, *47*, 558.
(22) Blöchl, P. E. *Phys. Rev. B* **1994**, *50*, 17953.
(23) Kresse, G.; Joubert, D. *Phys. Rev. B* **1999**, *59*, 1758.
(24) Ceperley, D. M.; Alder, B. J. *Phys. Rev. Lett.* **1980**, *45*, 566.
(25) Lamparth, I.; Nuber, B.; Schick, G.; Skiebe, A.; Grösser, T.; Hirsch, A. *Angew. Chem., Int. Ed.* **1995**, *34*, 2257.
(26) Yu, R.; Zhan, M.; Cheng, D.; Yang, S.; Liu, Z.; Zheng, L. *J. Phys. Chem.* **1995**, *99*, 1818.
(27) Henkelman, G.; Jonsson, H. *J. Chem. Phys.* **2000**, *113*, 9978.
(28) Jónsson, H. *Annu. Rev. Phys. Chem.* **2000**, *51*, 623.
(29) Henkelman, G.; Uberuaga, B. P.; Jonsson, H. *J. Chem. Phys.* **2000**, *113*, 9901.
(30) Sanville, E.; Kenny, S. D.; Smith, R.; Henkelman, G. *J. Comput. Chem.* **2007**, *28*, 899.
(31) Kaukonen, M.; Kujala, R.; Kauppinen, E. *J. Phys. Chem. C* **2011**, *116*, 632.